NM WRRI Student Water Research Grant Final Report

1.Student researcher: Dulith Rajapakshe, Department of Civil Engineering, New Mexico State University, Las Cruces, New Mexico, 88003
Faculty advisor: Dr. Runwei Li, Department of Civil Engineering, New Mexico State University, Las Cruces, New Mexico, 88003

2. Project title: Co-transport of perfluorooctane sulfonic acid (PFOS) and its novel alternatives 8:2 chlorinated polyfluorinated ether sulfonate (8:2 CL-PFESA) F53B in saturated silicon columns

3. Description of research problem and research objectives.

Research Problem and Objectives:

Perfluorooctane sulfonate (PFOS), with the chemical formula $C_8F_{17}SO_4$, is a type of per- and polyfluoroalkyl substance (PFAS) commonly used in products such as polishing agents, non-stick coatings, cleaning supplies, fire-fighting foams, and electroplating (Paul et al., 2009). PFOS is widely dispersed in the environment and has been detected in humans. Due to its toxicity and extensive presence, its use was restricted starting in 2009 (Liu et al., 2017).

A newer compound, 9-chlorinated polyfluorinated ether sulfonate (9Cl-PF3ONS), also known as F53B ($C_8F_{18}ClSO_4K$), is used as a substitute for PFOS in the chrome plating industry. Due to its effectiveness, the use of F53B has increased, leading to higher levels of this substance in the environment. It has also been detected in human body fluids such as serum, breast milk, and urine, with concentrations of 530 ppb, 976 ppb, and 2860 ppb, respectively (Liu et al., 2021). Because of their chemical and biological inertness, PFOS and F53B are ubiquitous and persistent in the environment (Qi L et al., 2022). The unique amphiphilic properties and structural variations of PFAS make their adsorption processes complex, particularly during partitioning to solid matrices. Their hydrophobic fluorinated chains favor interactions with soil organic carbon, whereas their polar head groups readily associate with polar surface functionalities. This dual interaction capacity enables PFAS to attach both to organic matter and to oppositely charged mineral surfaces (Sundstrom et al., 2012). Reported PFAS concentrations in soil and sediments are several magnitudes higher than in groundwater (Brusseau et al., 2020). Gaining insight into the fate, transport, and exposure pathways of PFAS in subsurface environments is essential for informing strategies in environmental monitoring, risk evaluation, and the development of effective restoration and remediation approaches (Evich et al., 2022).

Their presence in soil and groundwater raises significant concerns regarding potential human health risks through various exposure routes. To accurately assess these risks and develop effective remediation strategies, it is crucial to thoroughly understand how PFAS are retained and transported

in the subsurface (Brusseau et al., 2019). Typically, the standard method for studying the retention and transport behavior of PFAS in the lab involves performing miscible displacement column experiments.

The partitioning mechanisms of PFOS and F53B are affected by their physicochemical properties, such as chain length, functional group, polarity, ion exchange state, and chain structure. Many studies have pointed out that electrostatic attraction, hydrophobic interaction, ligand exchange, and hydrogen bonding may also contribute to the partitioning mechanism (Du et al., 2014). Aligned with US EPA goal number 4, our research teams have focused on introducing granular activated carbon (GAC) and surfactant-modified granular activated carbon (MGAC) into the column. Unmodified GAC has negative or neutral charges due to its surface characterization. Because of this, unmodified GAC and PFAS interactions are limited to hydrophobic or van der Waals interactions. However, the introduction of cationic surfactants to the surface of GAC has increased its positive charge on the surface. Because of its positive charge, PFAS have been interacting with MGAC with electrostatic attractions, hydrophobic interactions, and van der Waals interactions. This phenomenon will increase the GAC adsorption capacity, and it will be a cost-effective and sustainable approach towards PFAS (PFOS and F53B) management. This study aims to develop a CTAC-modified GAC adsorbent and evaluate its environmental remediation potential under transport scenarios. This study contains three specific objectives.
Objective 1: Characterization of unmodified and modified GAC.
Objective 2: Evaluate PFOS and F53B individual and co-transport in saturated columns.
Objective 3: Assess the remediation potential for applying GAC/MGAC as PFAS adsorbents.

4. Description of methodology employed.

4.1 Materials: Cetyltrimethyl ammonium chloride (CTAC, ≥ 95 %) was purchased from Tokyo Chemical Industry. The PFOS, F53B, and PFHxS (Perfluorohexane Sulfonate) standards were obtained from Accustandard, Inc. (New Haven, CT). The LC/MS Grade water and methanol were purchased from Fisher Scientific (Hampton, NH).

4.2 GAC Preparation and Characterization: A commercial GAC was obtained from the New Mexico Brackish Groundwater National Desalination Research Facility. The unmodified GAC were added to a cationic surfactant solution with CTAC concentration at 6 mmol/L, and the mixtures were stirred at 200 rpm at 85 °C for 2 h, followed by rinsing with deionized (DI) water three times and drying at 70 °C for 12 h.

The morphological and compositional analyses of the unmodified and CTAC-modified GAC (MGAC) were performed with a scanning electron microscope equipped with energy dispersive (SEM-EDS, S-3400N Type II X-ray spectroscopy, Hitachi High-Technologies Corp.). The surface

area and pore volume of the adsorbents will be determined by a Brunauer−Emmett−Teller Analyzer (BET analyzer, ASAP 2050, Shimadzu). Chemical bonding structure was evaluated with (IRSprit X series FTIR, Shimadzu).

4.3 Column Study: In the following setup, 3 pore volumes (19.35 mL ×3) of PFOS, F53B, or PFOS and F53B mixture was injected into the column. Then 5 pore volumes of pure water were injected. After that, all the effluents were collected according to one-fourth of the pore volume time, approximately 9.50 min intervals, using a fraction collector (F203B Gilson Inc). The column was filled with five different scenarios, including (1) Sand only, (2) Sand with 5% GAC, (3) Sand with 5% MGAC, (4) Sand with 1% GAC, and (5) Sand with 1% MGAC. The percentage of GAC/MGAC addition was estimated according to total column volume. In different column conditions, porosity of the materials was evaluated at a constant level value of 0.50, which was used as the porosity in simulation. For each condition, PFOS, F53B individual runs and mixture run were conducted.

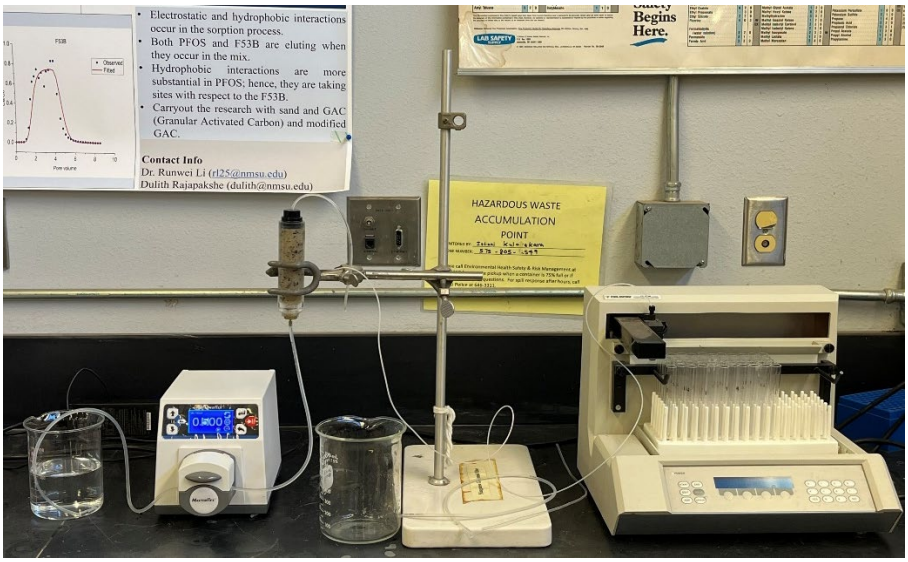

Figure 1- Column study setup

Table 1 - Column parameters.

Parameter	Length	Diameter	Volume	Flowrate	Porosity	Pore velocity	Hydraulic residence time
Value	10.4 cm	2.177 cm^2	38.71 cm^3	0.5 mL/min	0.5 (-)	16.11 cm/hr	0.64 hr

4.4 PFAS quantification: PFAS were quantified using a Shimadzu LC/MS 8050 quadrupole mass spectrophotometer, using an adapted EPA method 1633A. Agilent ACQUITY BEH C18 column (2.1 mm i.d, 100 mm length, 1.7 µm was used as the analytical column. During the quantification period, the column temperature was kept at 40 °C. Two mobile phases have been used for the

extraction: phase A with 2mM ammonium acetate in methanol and phase B with 2mM ammonium acetate in water. Table 2 represents the method conditions used in LC/MS 8050 (EPA, 2022)

Table 2 - LC/MS work conditions.

	Time (min)	**Flow (ml/min)**	**Phase A Conc.(%)**	**Phase B Conc.(%)**
1		0.800	90.0	10.0
2	1.00	0.800	90.0	10.0
3	3.00	0.800	1.0	99.0
4	3.01	0.800	1.0	99.0
5	5.00	0.800	1.0	99.0
6	5.01	0.800	90.0	10.0

4.5 Model Fitting using CXTIFIT: The one-dimensional steady-state equilibrium convection dispersion equation (CDE) used for the non-reactive tracer fitting

$$R\frac{\partial C}{\partial t} = D\frac{\partial^2 C}{\partial x^2} - v\frac{\partial C}{\partial x} + Rxn \quad (1)$$

Two sites, chemical nonequilibrium transport models, were used to fit PFOS, F53B and PFOS/F53B co-transport

$$\beta R\frac{\partial C_1}{\partial T} = \frac{1}{p}\frac{\partial^2 C_1}{\partial Z^2} - \frac{\partial C_1}{\partial Z} - \omega(C_1 - C_2) - \mu_1 C_1 \quad (2)$$

$$(1-\beta)R\frac{\partial C_2}{\partial T} = \omega(C_1 - C_2) - \mu_2 C_2 \quad (3)$$

where C_1 and C_2 are the dimensionless PFAS concentration in the solution and on the soil surface; β is the partition coefficient; ω is a dimensionless mass transfer coefficient; R is the retardation factor (R = 1+ $\rho_b \frac{K_d}{\theta}$, where ρ_b is the media bulk density, k_d is the partition coefficient between the solution and media, and θ is the porosity); T is the dimensionless time; P is the Peclet number (P= $\frac{vL}{D}$, where v is the interstitial pore-water velocity, L is the length of the column); D is the dispersion coefficient; μ_1 and μ_2 are the dimensionless deposition coefficients in the solution and on the soil surface (Toride et al., 1995).

5. Results and Discussion

5.1 GAC and MGAC characterization

5.1.1 SEM characterization

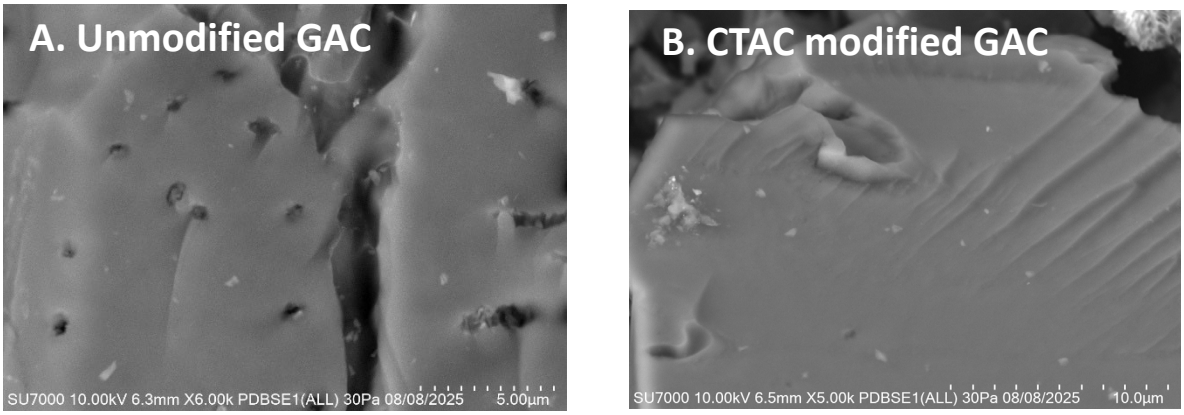

Figure 2 - A: Unmodified GAC and B: Modified GAC

Image A shows a fractured surface with often few pores. This observation was similar in the GAC surface, where it contains larger and smaller pores blended with a rough surface. Image B shows the MGAC surface, which contains a smooth surface without pores and fractures. Similar morphology can be observed in 50% the MGAC surface, but all the other spaces contain a similar GAC surface with pores and fractures.

5.1.2 BET characterization

Table 3 - BET surface characterization

Sample	Specific Surface Area (m^2/g)	Pore volume (cm^3/g)	Average pore width (Angstrom, Å)
GAC	687.08	0.183	49.78
MGAC	518.47	0.138	43.73

BET results have confirmed the morphological observation in SEM. BET clearly maps that GAC has a higher surface area compared to MGAC. The surface area decrement in MGAC is 25%. This is mainly because of the coating surface. It filled the pores with CTAC coating. Similar to surface area, pore volume also decreases by 25% from its original value. However, the average pore width decrement is not comparatively larger but only by 12.5%. So, both SEM and BET results confirmed the CTAC coating on the surface of MGAC.

5.1.3 FTIR characterization

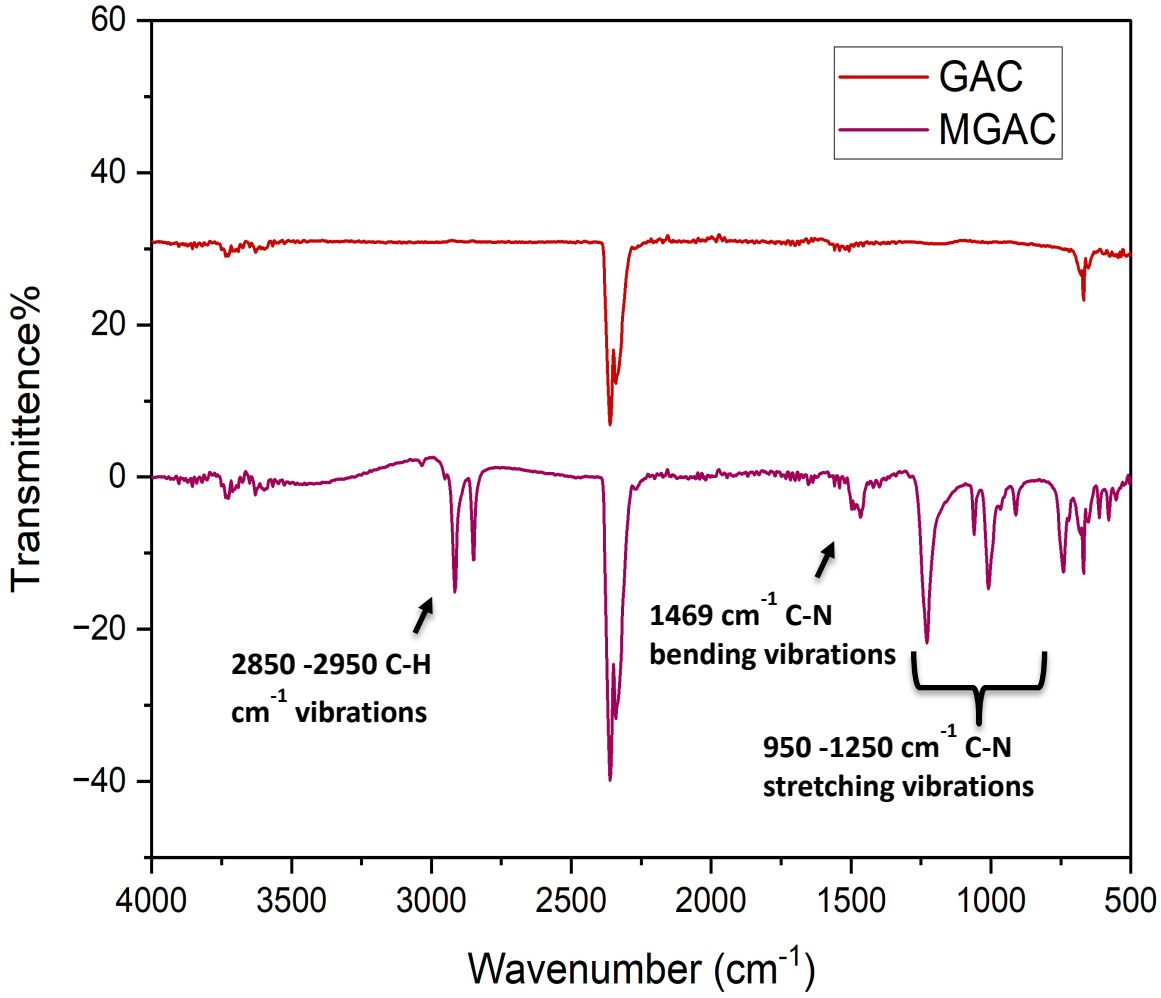

Figure 3 - FTIR spectrum of GAC and MGAC

The FTIR spectrum contains chemical characterizations of the GAC and MGAC. The MGAC spectrum contains numerous different peaks, compared to the GAC IR spectrum, which shows that MGAC has a chemically altered structure. The peaks observed at 2850 – 2950 cm^{-1} represent the C-H bending vibrations. That set of peaks came from the long hydrocarbon chain of the CTAC surfactant molecule. The one peak at 1469 cm^{-1} represents the C-N bending vibrations, which come from quaternary ammonium groups in the CTAC molecule. The peaks at 950 – 1250 cm^{-1} also represent the C-N stretching vibrations coming from quaternary ammonium groups in the CTAC molecule (Rivera et al., 2021).

5.2 Non-reactive tracer fitting

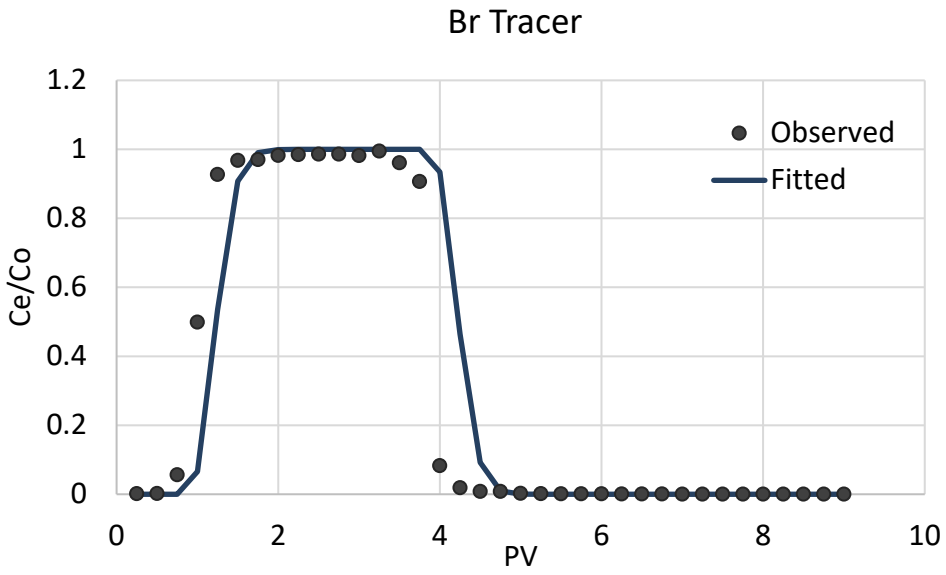

Figure 4 - Tracer fitting

NaBr was selected as a non-reactive tracer since there is GAC and MGAC. Bromide retention in the organic medium is relatively less compared to other groups. Tracer fitting gives 3.19 for the dispersion coefficient and 26 for the Peclet number. These values were used for the two-site model to fit the observed data.

5.3 PFAS Transport – Species Difference

5.3.1 PFAS Individual Transport in Sand

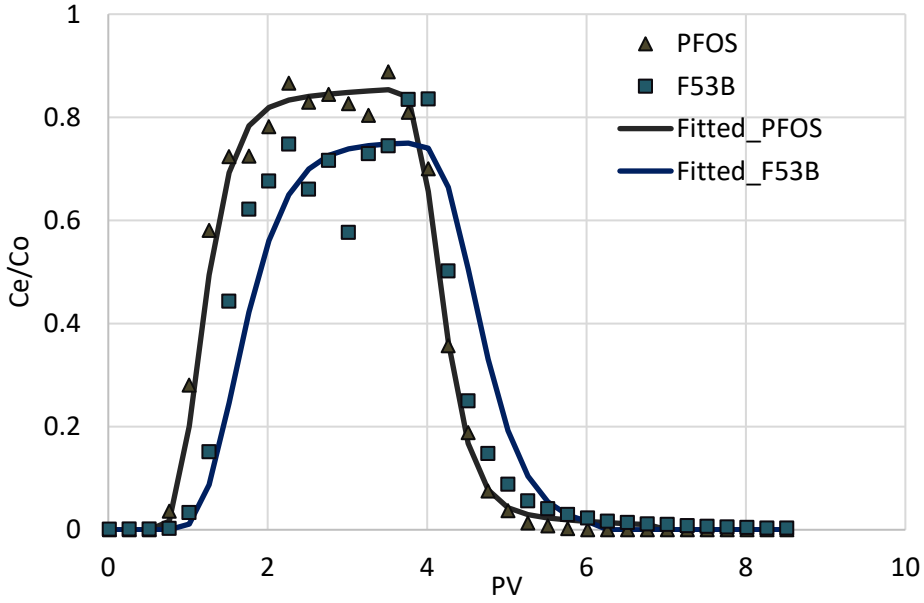

Figure 5 - PFAS individual transport in sand

As in Figure 5, the F53B breakthrough curve (BTC) is slightly skewed to the right side by highlighting possible retardation to the sand. PFOS has eluted with less retardation to the sand. Normally, sand has a negative impact on the surface. Both PFOS and F53B have negative charge ions. So, they tend to repel from each other without retaining. But PFAS chemicals have long hydrocarbon chains with hydrophobicity. Sand also contains hydrophobic places on the surface. During transportation, PFAS chemicals can be retained in those places that perform hydrophobic interactions. F53B has more hydrophobicity due to its higher molecular weight, so it might tend to retain on the sand compared to PFOS. In general, chain length increment might be responsible for the higher hydrophobicity (Guelfo et al., 2020; Nguyen et al., 2020). In the current observation, PFOS has little retardation compared to F53B. According to the fitted parameters, PFOS and F53B recoveries are 86% and 75% respectively. These values confirmed that F53B has remained inside of the column. Retardation factor of 1.58 in F53B confirmed the skewness towards the right side in F53B. PFOS has a partition coefficient of 0.90, which suggests that most of the PFOS is going through to equilibrium sites. Equilibrium sites often have adsorption and desorption at the same time. While F53B has 0.625, this suggests that compared to equilibrium adsorption, it is going to the non-equilibrium sites, where it adsorbs and desorbs slowly, likely as kinetic adsorption. Adsorption in non-equilibrium sites shows higher retardation. The mass transfer coefficient shows the rate of non-equilibrium reaction of that particular adsorbent.

Table 4 - Fitted parameters on PFAS individual transport in sand

Fitted Parameters	PFOS	F53B
Partition coefficient (β)	0.905	0.625
Mass transfer coefficient (ω)	0.06	2.25
Degradation factor (μ)	0	0
Retardation factor (R)	0.98	1.58
Recovery	86.5%	74.9%
R^2	0.95	0.96

5.3.2 PFAS co-transport in Sand

In the co-transport scenario, PFAS compounds have higher recovery rates compared to their individual runs. PFOS recovery has increased to 89% and surprisingly, F53B recovery went to 86% from 75%. By looking at the breakthrough curve, it clearly implies that both have good shape BTCs. The long tails that could be seen in individual transport have been diminished. However, in the retardation factor values, F53B still has a higher value compared to PFOS. B value for PFOS is now decreased, and more solutes adsorb to the non-equilibrium sites compared to their individual transport. This may be due to limited equilibrium sorption sites. Some sites were occupied because of F53B and PFOS, which tend to react with non-equilibrium sites. F53B has a similar β value, but

its reaction rate has decreased from 2.25 to 0.940, suggesting kinetic adsorption is a little faster compared to its single run. In both PFAS compounds, mass transfer coefficient values are less than 1, indicating that reaction rates for the non-equilibrium sites are a little faster. This scenario improves the BTC shape by adjusting the retardation factor close to 1.

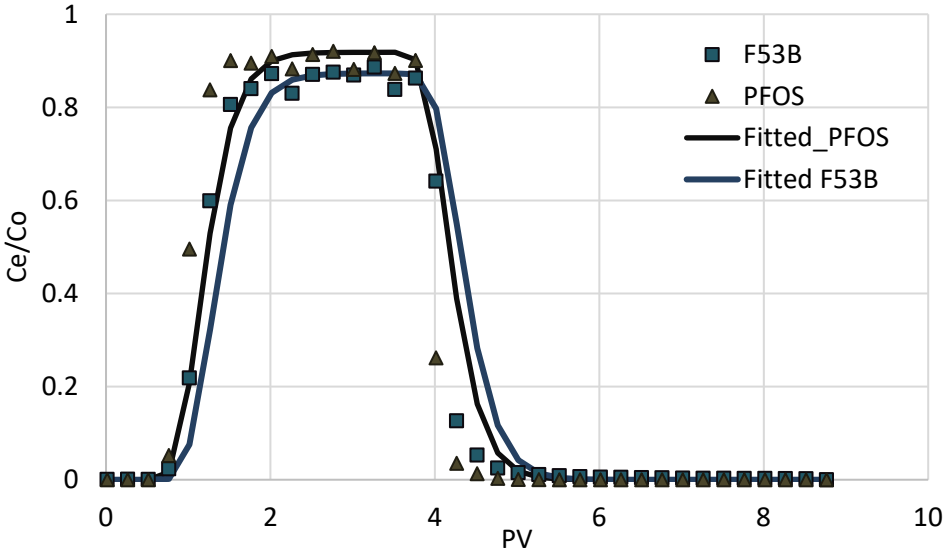

Figure 6- Co-transport of PFOS and F53B mix in sand

Table 5 - Fitted parameters of PFOS and F53B co-transport in sand

Fitted parameters	PFOS mix	F53B mix
Partition coefficient (β)	0.851	0.679
Mass Transfer Coefficient (ω)	0.785	0.940
Degradation factor (μ)	0.08	0
Retardation factor (R)	0.98	1.17
Recovery	89.10%	85.97%
R^2	0.99	0.98

5.4 GAC impact on PFAS transportation

5.4.1 PFAS individual transport with 5% GAC

GAC is known to be PFAS adsorptive material. Introduction of GAC into the column blended with sand represents the PFAS mitigation as well as the transport scenario. In BTC recoveries of both PFOS and F53B have dropped to 7.25% and 6.58% respectively. Compared to sand GAC has preferred adsorption sites. Looking at the BTC, both curves are similar to each other yet, F53B shows slight retention by the tail. According to fitting parameters, similar to sand, PFOS has preferred equilibrium and F53B has preferred non-equilibrium sites compared to PFOS. However,

PFOS now has slightly higher mass transfer coefficient compared to sand transport. This implies portions that prefer non-equilibrium sites have a kinetic reaction rate. This is the reason why both curves have similar shapes.

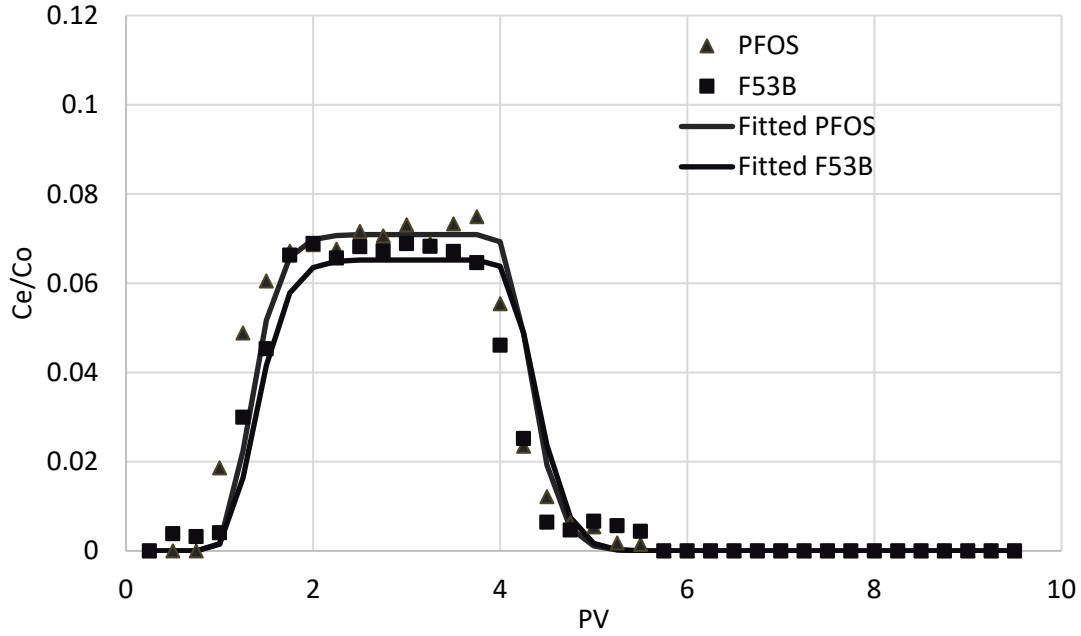

Figure 7 - Individual transport of PFOS and F53B in 5% GAC

Table 6 - Fitted parameters for individual transport of PFOS and F53B in 5% GAC

Fitted Parameters	**PFOS**	**F53B**
Partition coefficient (β)	0.919	0.625
Mass Transfer Coefficient (ω)	1.062	2.25
Degradation factor (μ)	2.72	2.61
Retardation factor (R)	1.23	1.29
Recovery	7.25%	6.58%
R^2	0.99	0.98

5.4.2. PFAS co-transport with 5% GAC

Similar to sand, both PFOS and F53B recovery rates were higher compared to their individual transport run. Both PFOS and F53B compounds contain similar β values, and they have settled with similar ω values. Because of these similar values, their retardation values are similar to each other. According to the values, when they are transported together as a mixture, they tend to copy each other's behavior to adsorption sites and reaction rates. This can mainly happen due to the competition between two chemicals for the limited adsorption sites. However, this is different

compared to co-transport in sand, because in the 5%GAC run, there are more adsorption sites compared to sand.

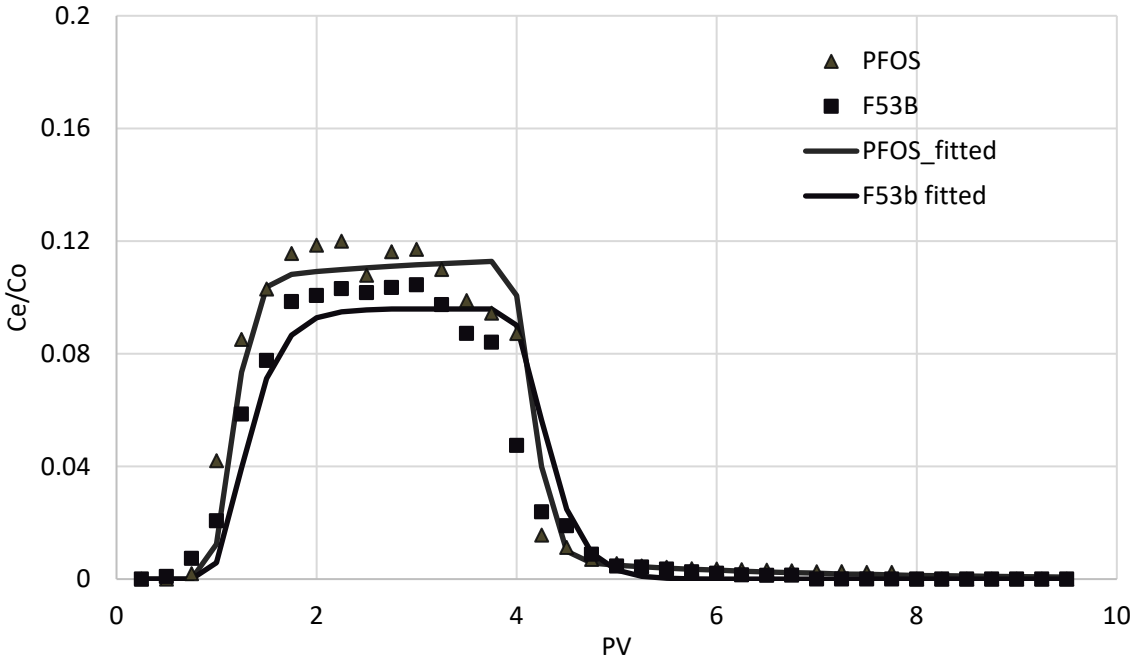

Figure 8 - Co-transport of PFOS and F53B in 5% GAC

Table 7 - Fitting parameters of Co-transport of PFOS and F53B in 5% GAC

Fitted Parameters	**PFOS mix**	**F53B mix**
Partition coefficient (β)	0.827	0.84
Mass Transfer Coefficient (ω)	1.04	1.41
Degradation factor (μ)	2.31	2.43
Retardation factor (R)	1.20	1.31
Recovery	11.60%	9.71%
R^2	0.97	0.99

5.5 MGAC vs GAC

5.5.1 PFAS co-transport in 1% GAC

In the shifting process from 5% GAC to 1% GAC, recoveries of both PFOS and F53B have increased by 7 folds. When a limited GAC is present, it favors the retention of F53B. This scenario can be observed in the BTCs, where the F53B curve is slightly skewed to the right. The fitted model tells that β values for both PFAS compounds are similar, and they prefer equilibrium adsorption sites compared to non-equilibrium sites. Both β and ω values confirm the retardation of F53B. The values of β increased due to the limited adsorption sites, and because of less GAC, the complexity of the transport medium is less obvious.

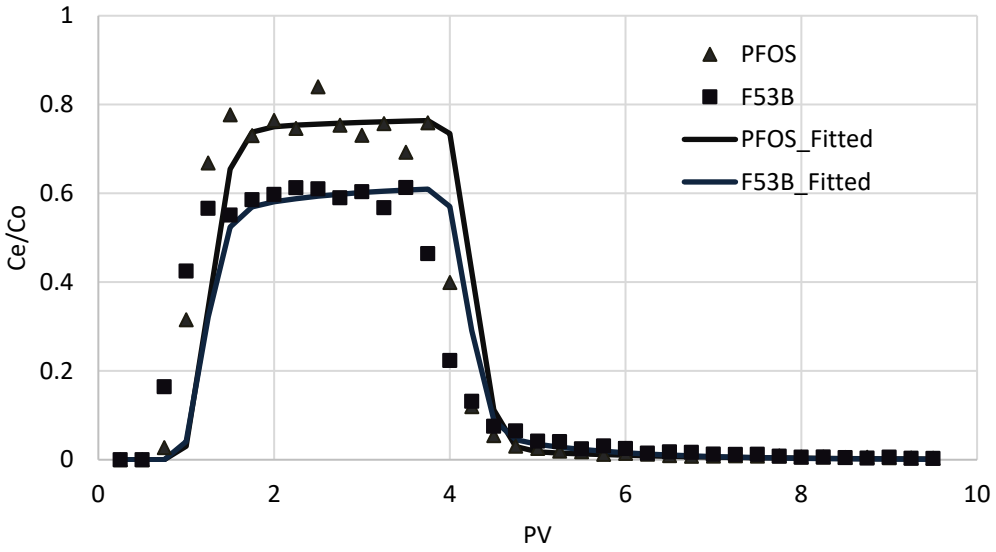

Figure 9 - Co-transport of PFOS and F53B in 1% GAC

Table 8 - Fitted parameters of Co-transport of PFOS and F53B in 5% GAC

Fitted Parameters	**PFOS**	**F53B**
Partition coefficient (β)	0.99	0.98
Mass Transfer Coefficient (ω)	0.04	0.11
Degradation factor (μ)	0.25	0.48
Retardation factor (R)	1.08	1.15
Recovery	77.87%	64.36%
R^2	0.99	0.98

5.5.2 PFAS individual transport in 1% GAC

Individual transport of PFOS and F53B has similar patterns to the co-transport of both species. However, recovery percentage values were less than those of the co-transport scenario. This is

guaranteed since there is no competition between PFOS and F53B for the GAC sites. As expected, F53B still possesses higher retention compared to PFOS in GAC sites.

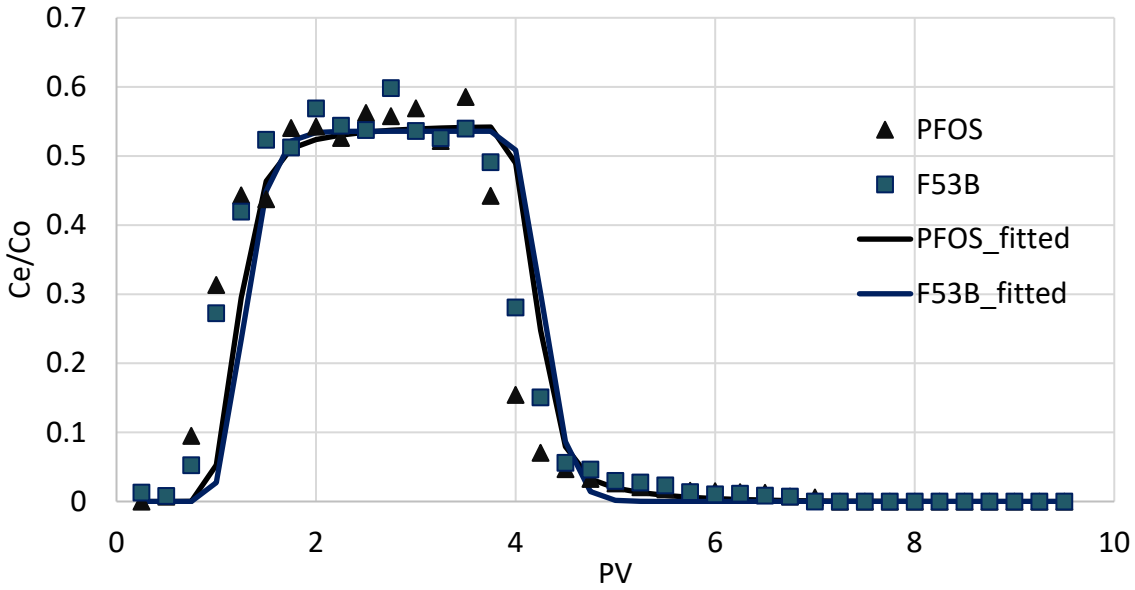

Figure 10-Individual transport of PFOS and F53B in 1% GAC

T

Fitted Parameters	PFOS	F53B
Partition coefficient (β)	0.936	0.934
Mass Transfer Coefficient (ω)	0.113	0
Degradation factor (μ)	0.617	0.632
Retardation factor (R)	1.07	1.18
Recovery	54.87%	56.67%
R^2	0.98	0.99

5.5.3 PFAS co-transport in 1% MGAC

In this study, 5% MGAC is also used in the column, and it tends to absorb all the PFOS and F53B in contamination. This obstructs the construction of both BTC of PFOS and F53B. However, 1% MGAC absorbed more than 90% of PFOS and F53B. MGAC changes the transportation behavior that was observed in sand, 5% GAC, and 1% GAC. Both PFOS and F53B BTC have a skewed right side by leaving a long tail. According to this specific shape, it can suggest that adsorption of MGAC is kinetic adsorption, where adsorption happens at slower rates. β values are less than 0.50

for both compounds, suggesting adsorption into non-equilibrium sites compared to equilibrium sites. Mass transfer coefficient values are greater than 3 for both compounds, and it confirms the kinetic adsorption of PFAS onto the MGAC surface. Retardation factors for the PFOS and F53B are 3.32 and 3.65, respectively. According to the fitted data and observations, the modification process from CTAC has clearly altered the surface of GAC, and it has altered the transport behavior compared to sand and GAC medium.

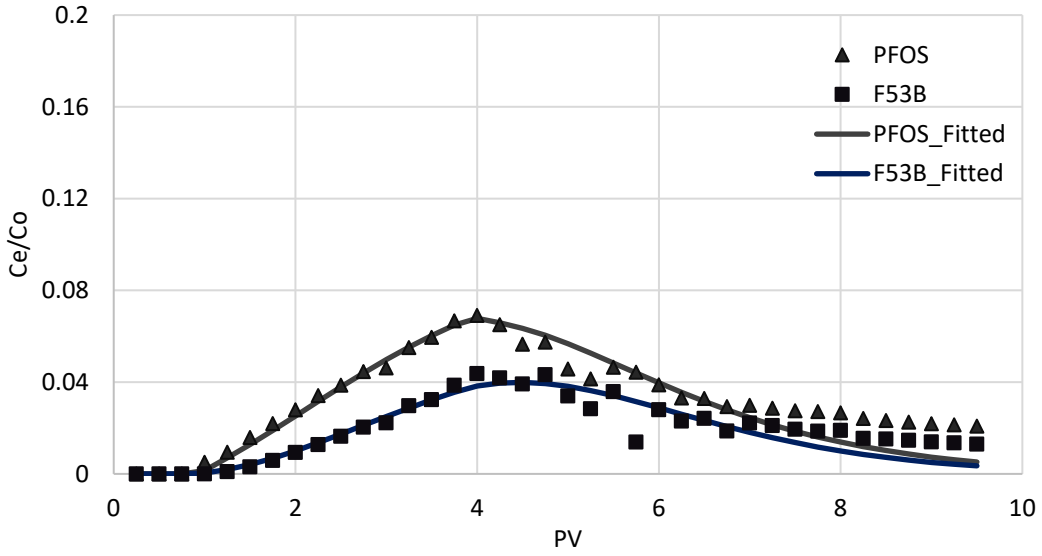

Figure 11- Co-transport of PFOS and F53B in 1% MGAC

Table 9 - Fitted parameters of PFOS and F53B in 1% MGAC

Fitted Parameters	PFOS mix	F53B mix
Partition coefficient (β)	0.303	0.274
Mass Transfer Coefficient (ω)	5.060	3.39
Degradation factor (μ)	2.92	2.41
Retardation factor (R)	3.32	3.65
Recovery	10.05%	5.98%
R^2	0.81	0.80

5.5.4 PFAS individual transport in 1% MGAC

Clearly, individual transportation also emphasizes that F53B and PFOS pose a kinetic adsorption equilibrium with modified GAC. However, according to the fitted parameters, we could clearly see there are higher recoveries for both species. Adsorption-wise, co-transport of both species fond of attracting into the surface, while individual transportation slightly hesitates, with the previous

statement showing lower retardations and higher recoveries. Even though F53B still absorbs more onto the surface rather than PFOS. One assumption would be that, since the ionic strength of the solution media is less due to the individual transport, species tend to elute more efficiently compared to co-transportation phenomena.

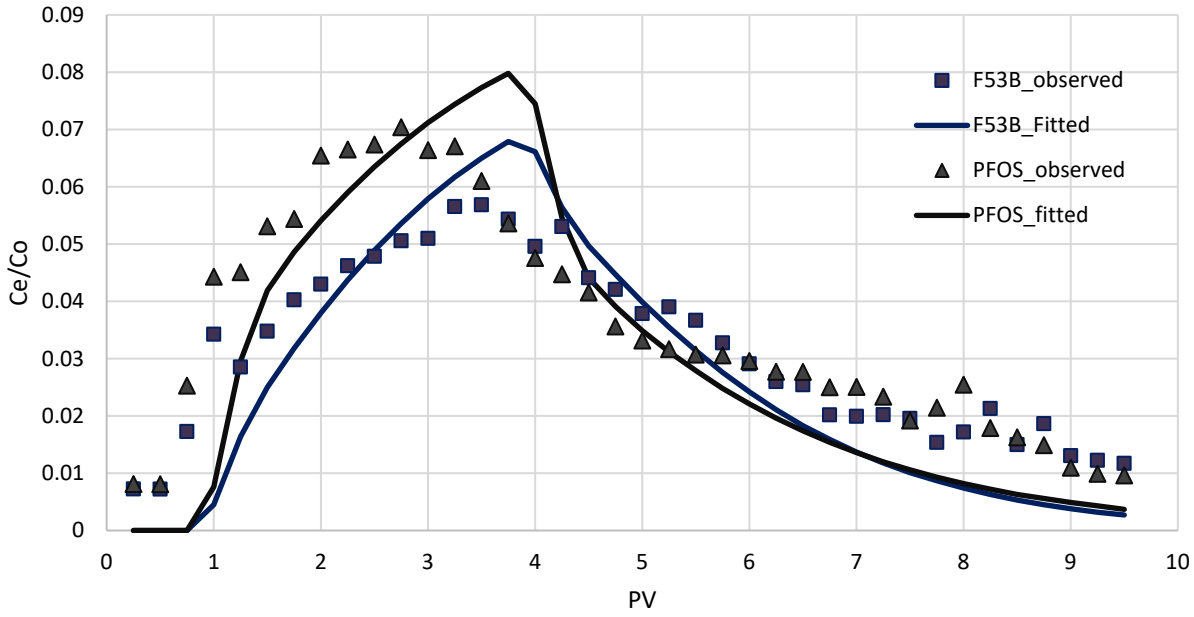

Figure 12 - Individual transport of PFOS & F53B in 1% MGAC

Table 10 - Fitted parameters of PFOS and F53B individual transport in 1% MGAC

Fitted Parameters	**PFOS**	**F53B**
Partition coefficient (β)	0.403	0.373
Mass Transfer Coefficient (ω)	1.206	2.00
Degradation factor (μ)	2.46	2.63
Retardation factor (R)	2.42	2.58
Recovery	11.05%	9.98%
R^2	0.77	0.72

5.6 Conclusions

- CTAC modification – CTAC coating alters the surface characteristics of GAC as well as PFAS interaction, indicated by surface analysis and different transport patterns.

- Chemical-dependent transport: In each scenario, F53B has higher retention compared to PFOS with lower recovery rates. The observation suggests F53B has higher hydrophobic interactions compared to PFOS, which may be due to either its linkage or higher molecular weight.
- Co-occurrence impact on transport: Both PFOS and F53B show higher recoveries and similar retardation factors when co-transporting compared to individual runs, suggesting the competition between these two PFOS species.
- MGAC Effectiveness in PFAS retaining: Among all GAC/MGAC amended transport scenarios, 1% MGAC has led to the most profound retardation for PFOS and F-53B, as compared to 5% and 1% GAC.

5.7 References

Brusseau, M. L., Anderson, R. H., & Guo, B. (2020). PFAS concentrations in soils: Background levels versus contaminated sites. *Science of the Total environment*, *740*, 140017.

Brusseau, M. L., Khan, N., Wang, Y., Yan, N., Van Glubt, S., & Carroll, K. C. (2019). Nonideal transport and extended elution tailing of PFOS in soil. *Environmental science & technology*, *53*(18), 10654–10664.

Du, Z., Deng, S., Bei, Y., Huang, Q., Wang, B., Huang, J., & Yu, G. (2014). Adsorption behavior and mechanism of perfluorinated compounds on various adsorbents—A review. *Journal of hazardous materials*, *274*, 443–454.

EPA, U. (2022). *Method 1633, Revision A Analysis of Per- and Polyfluoroalkyl Substances (PFAS) in Aqueous, Solid, Biosolids, and Tissue Samples by LC-MS/MS ;* . https://www.epa.gov/system/files/documents/2024-12/method-1633a-december-5-2024-508-compliant.pdf

Evich, M. G., Davis, M. J., McCord, J. P., Acrey, B., Awkerman, J. A., Knappe, D. R., Lindstrom, A. B., Speth, T. F., Tebes-Stevens, C., & Strynar, M. J. (2022). Per-and polyfluoroalkyl substances in the environment. *Science*, *375*(6580), eabg9065.

Guelfo, J. L., Wunsch, A., McCray, J., Stults, J. F., & Higgins, C. P. (2020). Subsurface transport potential of perfluoroalkyl acids (PFAAs): Column experiments and modeling. *Journal of Contaminant Hydrology*, *233*, 103661.

Liu, S., Lai, H., Wang, Q., Martínez, R., Zhang, M., Liu, Y., Huang, J., Deng, M., & Tu, W. (2021). Immunotoxicity of F53B, an alternative to PFOS, on zebrafish (Danio rerio) at different early life stages. *Science of the Total environment*, *790*, 148165.

Liu, Y., Ruan, T., Lin, Y., Liu, A., Yu, M., Liu, R., Meng, M., Wang, Y., Liu, J., & Jiang, G. (2017). Chlorinated polyfluoroalkyl ether sulfonic acids in marine organisms from Bohai Sea, China: occurrence, temporal variations, and trophic transfer behavior. *Environmental science & technology*, *51*(8), 4407–4414.

Nguyen, T. M. H., Bräunig, J., Thompson, K., Thompson, J., Kabiri, S., Navarro, D. A., Kookana, R. S., Grimison, C., Barnes, C. M., & Higgins, C. P. (2020). Influences of chemical properties, soil properties, and solution pH on soil–water partitioning coefficients of per- and polyfluoroalkyl substances (PFASs). *Environmental science & technology*, *54*(24), 15883–15892.

Paul, A. G., Jones, K. C., & Sweetman, A. J. (2009). A first global production, emission, and environmental inventory for perfluorooctane sulfonate. *Environmental science & technology*, *43*(2), 386–392.

Rivera, G. L. D., Hernández, A. M., Cabello, A. F. P., Barragán, E. L. R., Montes, A. L., Escamilla, G. A. F., Rangel, L. S., Vazquez, S. I. S., & Del Río, D. A. D. H. (2021). Removal of chromate anions and immobilization using surfactant-modified zeolites. *Journal of Water Process Engineering*, *39*, 101717.

Sundstrom, S. M., Allen, C. R., & Barichievy, C. (2012). Species, functional groups, and thresholds in ecological resilience. *Conservation Biology*, *26*(2), 305–314.

Toride, N., Leij, F., & Van Genuchten, M. T. (1995). *The CXTFIT code for estimating transport parameters from laboratory or field tracer experiments* (Vol. 2). version.

6. Provide a paragraph on who will benefit from your research results. Include any water agency that could use your results.

Hydrologists, scientists, and research students can use these data to understand how PFAS interact with GAC and MGAC. MGAC would be a suitable approach in permeable reactive barriers to control the PFAS contaminated plumes.

7. Describe how you have spent your grant funds.

Item	Amount	Justification
Salary		
Student PI	$3,282	1.5 summer month salary for the student PI at 0.5 FTE
Fringe Benefit		
Student PI	$16	0.50% fringe rate for student PI
Lab Supplies		
PFAS stock solutions	$325	F53B,PFOS and PFHxS stock solutions at a unit price of $150 and $175 will be purchased from Wellington LLC
Methanol - LCMS grade (1L×4)	$272	Two packs of LCMS grade methanol at a unit price of $138 (Fisher Scientific) for PFAS analysis
Water - LCMS grade (1L×6)	$420	Two packs of LCMS grade water at a unit price of $210 (Fisher Scientific) for PFAS analysis
Service		
LC/MS analysis	$2800	LC/MS will be used to quantify PFAS concentrations
Other		
Other Cost	$385	A budget of $385 will be used for other potential costs (e.g., printing posters and office supplies purchase)

8. List of presentations you have made related to the project.

Oral presentation at ACS Fall 2025 in Washington, DC under Advances of PFAS research and outlooks. (2025) Presentation title - Co-transport of perfluoro octane sulfonic acid (PFOS) and their novel alternatives 8:2 chlorinated polyfluorinated ether sulfonate (8:2 CL-PFESA) F53B in saturated silicon columns

WRRI conference 2024 held at Santa Fe.

9. List publications or reports, if any, that you are preparing. For all publications/reports and posters resulting from this award, please attribute the funding to NM WRRI and the New Mexico State Legislature by including the account number: NMWRRI-SG-FALL2024.

None at the moment, Looking forward to draft a paper from the findings.

10. List of any other students or faculty members who have assisted you with your project.

Dr.Runwei Li, Yun Ma, Lin Wang

11. Provide special recognition awards or notable achievements as a result of the research, including any publicity such as newspaper articles, or similar.

Got selected to ACS Fall 2025 as a oral presentation

12. Provide information on degree completion and future career plans. Funding for student grants comes from the New Mexico Legislature and legislators are interested in whether recipients of these grants go on to complete academic degrees and work in a water-related field in New Mexico or elsewhere.

I am currently pursuing a Ph.D. in Civil and Environmental Engineering and anticipate completing my degree in spring 2027. Post-graduation, I aim to deepen my involvement in research and development within either academic or industrial settings, focusing on complex challenges related to natural resources, energy systems, and the protection of human and environmental health. I am also open to opportunities in state or federal government agencies, where I can apply my interdisciplinary background to support the development and implementation of science-based environmental regulations that safeguard water, air, and land resources.